Passive Hierarchical Impedance Control Via Energy Tanks

Alexander Dietrich, Xuwei Wu, Kristin Bussmann, Christian Ott, Alin Albu-Schäffer, and Stefano Stramigioli

***Abstract*—Modern robotic systems with a large number of actuated degrees of freedom can be utilized to perform several tasks at the same time while following a given order of priority. The most frequently used method is to apply null space projections to realize such a strict hierarchy, where lower priority tasks are executed as long as they do not interfere with any higher priority objectives. However, introducing null space projectors inevitably destroys the beneficial and safety-relevant feature of passivity. Here, two controllers are proposed to restore the passivity: one with local energy tanks on each hierarchy level and one with a global tank for the entire system. The formal proofs of passivity show that no energy is generated by these controllers. Once the tanks are empty, passivity is still guaranteed at the cost of some control performance. Simulations and experiments on a torque-controlled robot validate the approaches and predestine them for the usage in safety-relevant applications.**

***Index Terms*—Compliance and impedance control, force control, motion control of manipulators, redundant robots.**

I. Introduction

KINEMATICALLY redundant robots have more actuated degrees of freedom (DOF) than necessary to perform a given task. These redundant DOF can be used to execute several additional tasks while following a strict hierarchy. In other words, tasks with lower priority may not disturb tasks with higher priority and are performed as well as possible under this restriction. The most frequent approach is to implement null space projections [1]–[3]. However, the projectors modify the energy flows in the system and destroy the precious and safety-critical property of passivity [4], [5].

So-called *energy tanks* are often utilized in various subdomains of robotics, e.g. in bilateral telemanipulation [6]–[9], if the energy flow in a system has to be altered in a deliberate way. In [10] the energy stored in the tank is exploited to compensate for position drift between master and slave during contact tasks, while passivity is preserved. A two-layer framework was proposed in [8], where the passivity layer is constructed of two tanks at both master and slave sides. Stable behavior in the presence of time-varying, destabilizing factors such as hard contacts or communication delays is guaranteed. A decentralized controller for a heterogeneous group of mobile robots was presented in [9]. The robots are treated at the slave side, while the human operator on the master side is equipped with force feedback devices. Tanks in each slave agent are employed to implement passivity-based techniques and guarantee system stability.

In impedance control, energy tanks are applied to reproduce time-varying stiffness [11]. While classical controllers cannot guarantee passivity due to generation of extra energy by the changing stiffness, the authors restore the passivity and ensure stable behavior. The strategy was further developed in [12] and used in an admittance controller with time-varying inertia, stiffness, and damping matrices. Furthermore, the formal description of a port-Hamiltonian system endowed with a tank is also given there. In [13] energy- and power-based safety metrics are used to limit both the injected energy and its power rate from the impedance controller to the system, which is achieved by varying the stiffness and the damping matrices. The desired output control torque is regulated by an energy tank to preserve the passivity. A hybrid force/impedance controller is developed in [14] to perform sensitive manipulation tasks in unmodeled environments. A tank element is introduced to deal with potentially non-passive terms. In [15] a damping design in velocity feedback control is used that selectively dissipates energy in directions perpendicular to the desired motion. When the dynamic system model is non-conservative, the passivity of the control framework is not guaranteed anymore. An energy tank is implemented to prevent this loss of passivity.

In [4] we have restored the passivity for null space compliance control. A single tank has been implemented, which was filled by the accumulated energy from the active damping on both levels. Here we extend this fundamental idea to hierarchies with an arbitrary number of priority levels to make it usable in relevant, multi-objective robotic applications. Two approaches are proposed, validated, and compared with the classical, non-passive controller: 1) the installation of local energy tanks on each hierarchy level, 2) the use of one global energy tank for the complete robot. Both solutions restore the passivity, yet they feature additional properties. Since their analysis and control design require an adequate representation of the hierarchical dynamics, we utilize the recently developed description from [16], [17]. The approaches are evaluated and compared in simulations as well as in experiments on the torque-controlled humanoid robot Rollin' Justin.

Manuscript received September 9, 2016; accepted December 18, 2016. Date of publication December 28, 2016; date of current version January 16, 2017. This paper was recommended for publication by Editor P. Rocco and Editor C. Gosselin upon evaluation of the reviewers comments. This work was supported by European Robotics Challenges under Grant CP-IP 608849.

A. Dietrich, K. Bussmann, and C. Ott are with the Institute of Robotics and Mechatronics, German Aerospace Center, Wessling 82234, Germany (e-mail: alexander.dietrich@dlr.de; kristin.bussmann@dlr.de; christian.ott@dlr.de).

X. Wu is with the Technical University of Munich, Munich 80805, Germany (e-mail: xuwei.wu@tum.de).

A. Albu-Schäffer is with the Institute of Robotics and Mechatronics, German Aerospace Center, Wessling 82234, Germany, and also with the Technical University of Munich, Munich 80805, Germany (e-mail: alin.albu-schaeffer@dlr.de).

S. Stramigioli is with the University of Twente, Enschede 7500AE, The Netherlands (e-mail: s.stramigioli@ieee.org).

Color versions of one or more of the figures in this letter are available online at http://ieeexplore.ieee.org.

Digital Object Identifier 10.1109/LRA.2016.2645504

The paper is organized as follows: after recapitulating the fundamentals in hierarchical control in Sect. II, the local-tank and global-tank approaches are introduced in Section III and Section IV, respectively. Proofs of passivity are given. Afterwards, simulations and experiments are conducted in Section V. The discussion in Section VI closes the paper.

II. Fundamentals

The dynamics of a robot with n DOF can be described by

$$\boldsymbol{M}(\boldsymbol{q})\ddot{\boldsymbol{q}} + \boldsymbol{C}(\boldsymbol{q},\dot{\boldsymbol{q}})\dot{\boldsymbol{q}} + \boldsymbol{g}(\boldsymbol{q}) = \boldsymbol{\tau} + \boldsymbol{\tau}^{\mathrm{ext}} \,, \tag{1}$$

where $\boldsymbol{q} \in \mathbb{R}^n$ describes the joint configuration. The inertia matrix $\boldsymbol{M}(\boldsymbol{q}) \in \mathbb{R}^{n\times n}$ is symmetric and positive definite, the Coriolis/centrifugal matrix $\boldsymbol{C}(\boldsymbol{q},\dot{\boldsymbol{q}}) \in \mathbb{R}^{n\times n}$ is formulated such that $\dot{\boldsymbol{M}}(\boldsymbol{q}) = \boldsymbol{C}(\boldsymbol{q},\dot{\boldsymbol{q}}) + \boldsymbol{C}(\boldsymbol{q},\dot{\boldsymbol{q}})^T$ holds. The generalized gravity forces are given by $\boldsymbol{g}(\boldsymbol{q}) \in \mathbb{R}^n$, the generalized forces $\boldsymbol{\tau} \in \mathbb{R}^n$ determine the control input, while $\boldsymbol{\tau}^{\mathrm{ext}} \in \mathbb{R}^n$ are the generalized external forces. In the following the dependencies on the states are omitted in the notations, if not strictly necessary for the understanding.

A control task hierarchy consisting of r priority levels with the respective task coordinates $\boldsymbol{x}_i = \boldsymbol{f}_i(\boldsymbol{q}) \in \mathbb{R}^{m_i}$ and the associated task dimensions $m_i \in \mathbb{N}$ (for $i = 1 \dots r$) is introduced.[1] The highest-priority level has index $i = 1$, the lowest one has index $i = r$. The operational space velocities on the individual hierarchy levels are described by the mappings via the Jacobian matrices $\boldsymbol{J}_i = \partial \boldsymbol{f}_i(\boldsymbol{q})/\partial \boldsymbol{q}$:

$$\dot{\boldsymbol{x}}_i = \boldsymbol{J}_i \dot{\boldsymbol{q}} \,. \tag{2}$$

All Jacobian matrices are assumed to be of full row-rank and the stacked version, the so-called augmented Jacobian matrix $(\boldsymbol{J}_1^T, \dots, \boldsymbol{J}_r^T)^T$, is non-singular. The goal of the hierarchical controller is that lower-priority tasks do not disturb any higher-priority tasks, neither statically nor dynamically [18], and they are performed as well as possible under this restriction.

A. Hierarchical Dynamics

This strict hierarchy can be expressed in the dynamic equations by an adequate coordinate transformation such as [17] which leads to the formulation

$$\boldsymbol{\Lambda}\dot{\boldsymbol{v}} + \boldsymbol{\mu}\boldsymbol{v} = \bar{\boldsymbol{J}}^{-T}\left(-\boldsymbol{g} + \boldsymbol{\tau} + \boldsymbol{\tau}^{\mathrm{ext}}\right) \tag{3}$$

with the *block-diagonal* inertia matrix $\boldsymbol{\Lambda} \in \mathbb{R}^{n\times n}$, the Coriolis/centrifugal matrix $\boldsymbol{\mu} \in \mathbb{R}^{n\times n}$, and the local, hierarchy-consistent task velocities $\boldsymbol{v}_i \in \mathbb{R}^{m_i}$ for $i = 1 \dots r$ following

$$\begin{pmatrix} \boldsymbol{v}_1 \\ \vdots \\ \boldsymbol{v}_r \end{pmatrix} = \begin{pmatrix} \bar{\boldsymbol{J}}_1 \\ \vdots \\ \bar{\boldsymbol{J}}_r \end{pmatrix} \dot{\boldsymbol{q}} = \bar{\boldsymbol{J}}\dot{\boldsymbol{q}} \,. \tag{4}$$

The hierarchy-consistent Jacobian matrices $\bar{\boldsymbol{J}}_i$ for $i = 1 \dots r$ can be stacked to obtain the invertible matrix $\bar{\boldsymbol{J}} \in \mathbb{R}^{n\times n}$. While the main task level is not restricted ($\bar{\boldsymbol{J}}_1 = \boldsymbol{J}_1$), all subtasks are described by $\bar{\boldsymbol{J}}_i = (\boldsymbol{Z}_i\boldsymbol{M}\boldsymbol{Z}_i^T)^{-1}\boldsymbol{Z}_i\boldsymbol{M} \in \mathbb{R}^{m_i\times n}$ for $i = 2 \dots r$, where the null space base matrices $\boldsymbol{Z}_i \in \mathbb{R}^{m_i\times n}$ fulfill $\boldsymbol{J}_j\boldsymbol{Z}_i^T = \boldsymbol{0}\ \forall j < i$. For consistency in the notations, $\boldsymbol{Z}_1 = (\boldsymbol{J}_1^{M+})^T$ is introduced, i.e. the dynamically consistent pseudoinverse $\boldsymbol{J}_1^{M+} = \boldsymbol{M}^{-1}\boldsymbol{J}_1^T(\boldsymbol{J}_1\boldsymbol{M}^{-1}\boldsymbol{J}_1^T)^{-1}$ [2]. The derivation of all terms is detailed in [16].

[1] To simplify the notations, $\sum_{i=1}^{r} m_i = n$ is assumed. Note that *all* subsequent statements (control law, proof of passivity) are valid for $\sum_{i=1}^{r} m_i > n$ w. l. o. g. Only the hierarchy-consistent task dimension on level r in the dynamically decoupled space changes from m_r to $n - \sum_{i=1}^{r-1} m_i$.

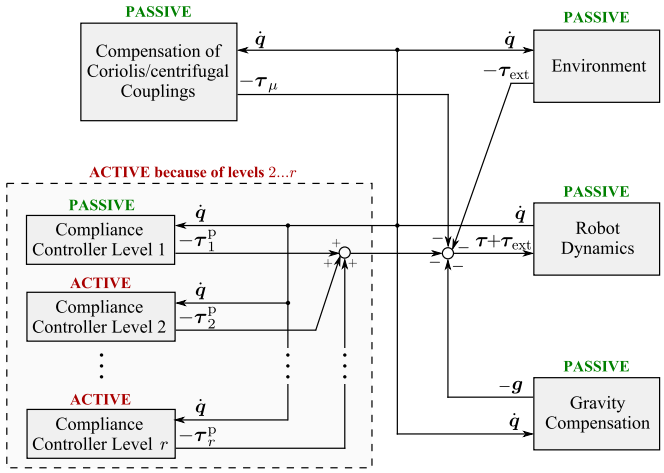

Fig. 1. Problem of activity in the classical controller. The closed loop is *no* interconnection of passive subsystems because the compliance controllers on all null space levels ($2 \dots r$) represent potentially active feedback actions.

B. Classical, Non-Passive Impedance Controller

The classical control law such as in [17] is

$$\boldsymbol{\tau} = \boldsymbol{g} + \boldsymbol{\tau}_\mu + \sum_{i=1}^{r} \underbrace{\bar{\boldsymbol{J}}_i^T\boldsymbol{Z}_i\boldsymbol{J}_i^T\boldsymbol{F}_i}_{\boldsymbol{\tau}_i^{\mathrm{p}}} \tag{5}$$

and contains the gravity compensation $\boldsymbol{g}$, the passive feedback action $\boldsymbol{\tau}_\mu \in \mathbb{R}^n$ to annihilate the remaining velocity-dependent Coriolis/centrifugal couplings across the priority levels, and the (null-space-projected) torques $\boldsymbol{\tau}_i^{\mathrm{p}}\ \forall i$ to perform all tasks in the hierarchy.[2] The control law is illustrated in Fig. 1. The operational space forces $\boldsymbol{F}_i \in \mathbb{R}^{m_i}$ on all levels $i = 1 \dots r$ are arbitrary and may, for example, realize desired spring-damper behaviors such as in a classical impedance controller [19]:

$$\boldsymbol{F}_i = -\left(\frac{\partial V_i(\tilde{\boldsymbol{x}}_i)}{\partial \boldsymbol{x}_i}\right)^T - \boldsymbol{D}_i\dot{\boldsymbol{x}}_i \,. \tag{6}$$

Herein, $V_i(\tilde{\boldsymbol{x}}_i)$ is the positive definite potential function describing such a spring with the error $\tilde{\boldsymbol{x}}_i = \boldsymbol{x}_i - \boldsymbol{x}_i^{\mathrm{d}}$, where $\boldsymbol{x}_i^{\mathrm{d}} \in \mathbb{R}^{m_i}$ is the desired value in the operational space for the regulation case, and $\boldsymbol{D}_i \in \mathbb{R}^{m_i\times m_i}$ is the damping matrix.

In the two-level case [4] we have shown that such a controller may generate active energy, thus the closed loop is *not passive*. Here, a task hierarchy with an arbitrary number of priority levels is considered, which is an active controller for the same reasons. The problem of activity due to the controller is sketched in Fig. 1. In the following, two energy-tank-based control approaches are introduced to restore the passivity and handle this safety-critical

[2] Note that $\bar{\boldsymbol{J}}_i^T\boldsymbol{Z}_i$ for $i = 2 \dots r$ can be interpreted as the dynamically consistent null space projector [2]. Moreover, on level 1, the simplification $\boldsymbol{\tau}_1^{\mathrm{p}} = \boldsymbol{J}_1^T\boldsymbol{F}_1$ can be made due to $\boldsymbol{Z}_1\boldsymbol{J}_1^T = \boldsymbol{I}$.

issue. The source of the activity will also be investigated and explained further in this context.

III. Controller With Local Energy Tanks

The joint velocities can be expressed as the sum of the contributions from all hierarchy levels [4], i.e.

$$\dot{\boldsymbol{q}} = \sum_{j=1}^{r} \boldsymbol{Z}_j^T \boldsymbol{v}_j \ . \tag{7}$$

Combining (2) and (7) yields

$$\dot{\boldsymbol{x}}_i = \underbrace{\boldsymbol{J}_i \sum_{j=1}^{i-1} \boldsymbol{Z}_j^T \boldsymbol{v}_j}_{\boldsymbol{w}_i} + \underbrace{\boldsymbol{J}_i \boldsymbol{Z}_i^T \boldsymbol{v}_i}_{\boldsymbol{\kappa}_i} \tag{8}$$

due to the annihilation $\boldsymbol{J}_i \boldsymbol{Z}_j^T = \boldsymbol{0}\ \forall j > i$. Therefore, $\dot{\boldsymbol{x}}_i$ can be expressed as the sum of two velocity components: $\boldsymbol{w}_i \in \mathbb{R}^{m_i}$ from all higher-priority levels and $\boldsymbol{\kappa}_i \in \mathbb{R}^{m_i}$ from level i itself. There are no contributions from the lower-priority levels $(i+1) \dots r$ in (8) thanks to the dynamic consistency in (3) and the *strictness* of the hierarchy.

A. Storage Function for Level i and Source of Activity

The virtual spring on level i is described by the potential function $V_i(\tilde{\boldsymbol{x}}_i)$, thus the storage function

$$S_{\mathrm{pot},i} = V_i(\tilde{\boldsymbol{x}}_i) \tag{9}$$

can be established. Using (8), its time derivative yields

$$\dot{S}_{\mathrm{pot},i} = \boldsymbol{\kappa}_i^T \left(\frac{\partial V_i(\tilde{\boldsymbol{x}}_i)}{\partial \boldsymbol{x}_i} \right)^T + \boldsymbol{w}_i^T \left(\frac{\partial V_i(\tilde{\boldsymbol{x}}_i)}{\partial \boldsymbol{x}_i} \right)^T \ . \tag{10}$$

The power transmission of the null space compliance controller w.r.t. the power port $(\dot{\boldsymbol{q}}, -\boldsymbol{\tau}_i^{\mathrm{p}})$ is

$$\begin{aligned} -\dot{\boldsymbol{q}}^T \boldsymbol{\tau}_i^{\mathrm{p}} &= \dot{\boldsymbol{q}}^T \bar{\boldsymbol{J}}_i^T \boldsymbol{Z}_i \boldsymbol{J}_i^T \left(\left(\frac{\partial V_i(\tilde{\boldsymbol{x}}_i)}{\partial \boldsymbol{x}_i} \right)^T + \boldsymbol{D}_i \dot{\boldsymbol{x}}_i \right) \\ &= \boldsymbol{\kappa}_i^T \left(\frac{\partial V_i(\tilde{\boldsymbol{x}}_i)}{\partial \boldsymbol{x}_i} \right)^T + \left(\dot{\boldsymbol{x}}_i - \boldsymbol{w}_i \right)^T \boldsymbol{D}_i \dot{\boldsymbol{x}}_i \end{aligned} \tag{11}$$

as $\dot{\boldsymbol{q}}^T \bar{\boldsymbol{J}}_i^T \boldsymbol{Z}_i \boldsymbol{J}_i^T = \boldsymbol{\kappa}_i^T$ holds. Inserting (11) into (10) yields

$$\begin{aligned} \dot{S}_{\mathrm{pot},i} &= -\dot{\boldsymbol{q}}^T \boldsymbol{\tau}_i^{\mathrm{p}} - \left(\dot{\boldsymbol{x}}_i - \boldsymbol{w}_i \right)^T \boldsymbol{D}_i \dot{\boldsymbol{x}}_i + \boldsymbol{w}_i^T \left(\frac{\partial V_i(\tilde{\boldsymbol{x}}_i)}{\partial \boldsymbol{x}_i} \right)^T \\ &= -\dot{\boldsymbol{q}}^T \boldsymbol{\tau}_i^{\mathrm{p}} - \dot{\boldsymbol{x}}_i^T \boldsymbol{D}_i \dot{\boldsymbol{x}}_i - \boldsymbol{w}_i^T \boldsymbol{F}_i \ . \end{aligned} \tag{12}$$

While the second term is obviously negative semi-definite for positive definite damping matrices $\boldsymbol{D}_i$, the sign of $-\boldsymbol{w}_i^T \boldsymbol{F}_i$ cannot be determined. This latter term induces a potentially non-passive feedback action of the null space compliance controller of level i w.r.t. $(\dot{\boldsymbol{q}}, -\boldsymbol{\tau}_i^{\mathrm{p}})$ and is the reason for the activity of these components in Fig. 1.

B. Introduction of Local Energy Tanks

In order to restore the passivity on the levels $i = 2 \dots r$, one virtual energy tank is placed on each hierarchy level storing the locally[3] dissipated energy of active damping. This feature can be interpreted as a passivity margin in an *integral sense* [20] and can be utilized to make the active subsystems in Fig. 1 passive such that the closed loop becomes an interconnection of exclusively passive subsystems.

The local energy tank is defined as a virtual storage element with flow variable $\dot{s}_i$ and effort variable s_i such that

$$E_{\mathrm{tank},i} = \frac{1}{2} s_i^2 \ . \tag{13}$$

In order to preserve the passivity even in case of an empty tank $(E_{\mathrm{tank},i} = 0)$, a new coordinate $\hat{\boldsymbol{x}}_i \in \mathbb{R}^{m_i}$ and its time derivative $\dot{\hat{\boldsymbol{x}}}_i \in \mathbb{R}^{m_i}$ are introduced from which the task torque on level i is generated. This variable $\hat{\boldsymbol{x}}_i$ may deviate from the original operational space coordinate $\boldsymbol{x}_i$ so as to keep the compliance controller subsystem for hierarchy level i passive at the cost of some control performance due to the deliberately introduced error $\hat{\boldsymbol{x}}_i - \boldsymbol{x}_i$. The new coordinate $\hat{\boldsymbol{x}}_i$ is the result of the numerical integration of

$$\dot{\hat{\boldsymbol{x}}}_i = \beta_i \underbrace{\left(\boldsymbol{w}_i + \boldsymbol{K}_{\mathrm{P},i} \left(\boldsymbol{x}_i - \hat{\boldsymbol{x}}_i \right) \right)}_{\hat{\boldsymbol{w}}_i} + \boldsymbol{\kappa}_i \tag{14}$$

w.r.t. time t. One can easily see the similarity to the original velocity $\dot{\boldsymbol{x}}_i$ in (8), yet two differences exist:

1) The term $\boldsymbol{K}_{\mathrm{P},i} \left(\boldsymbol{x}_i - \hat{\boldsymbol{x}}_i \right)$ with gain $\boldsymbol{K}_{\mathrm{P},i} \in \mathbb{R}^{m_i \times m_i}$ is introduced to reduce the drift and to let $\hat{\boldsymbol{x}}_i$ converge to $\boldsymbol{x}_i$ again. Incorporating this term leads to the introduction of the new velocity $\hat{\boldsymbol{w}} \in \mathbb{R}^{m_i}$.
2) The scalar β_i is introduced to control the tracking behavior of $\dot{\hat{\boldsymbol{x}}}_i$. If $\beta_i = 0$, then a deviation $\hat{\boldsymbol{x}}_i - \boldsymbol{x}_i \neq \boldsymbol{0}$ is deliberately induced. If $\beta_i = 1$, then $\lim_{t \to \infty} \left(\hat{\boldsymbol{x}}_i - \boldsymbol{x}_i \right) = \boldsymbol{0}$.

Parameter β_i can be interpreted as a *clutch* with two states:

$$\beta_i = \begin{cases} 0 & \text{if } E_{\mathrm{tank},i} \leq E_{\mathrm{tank},i}^{\min} \\ 1 & \text{else} \end{cases} \ . \tag{15}$$

To avoid discontinuities in (14), the transition between 0 and 1 can be made smooth such as in [15].[4] The new task force can be constructed based on $\hat{\boldsymbol{x}}_i$ and $\dot{\hat{\boldsymbol{x}}}_i$, where

$$\boldsymbol{F}_i = -\left(\frac{\partial V_i(\tilde{\hat{\boldsymbol{x}}}_i)}{\partial \hat{\boldsymbol{x}}_i} \right)^T - \boldsymbol{D}_i \dot{\hat{\boldsymbol{x}}}_i \tag{16}$$

replaces (6) and is applied in combination with (5). The new operational space error $\tilde{\hat{\boldsymbol{x}}}_i \in \mathbb{R}^{m_i}$ is defined as $\tilde{\hat{\boldsymbol{x}}}_i = \hat{\boldsymbol{x}}_i - \boldsymbol{x}_i^{\mathrm{d}}$.

C. Bond Graph and Energy Flows

The fill level of the tank must be limited to prevent a steady increase of the stored energy. Although large tank energy leads to a better control performance ($\beta_i = 1$), dangerous and aggressive behavior (e.g. large, undesired oscillations) of the robot could be tolerated and masked that way. Therefore, it is required to limit the maximum tank energy to a reasonable value, e.g. depending on the maximum allowed kinetic energy in the system. Fig. 2

[3]The term *local energy* indicates that the energy in the virtual tank remains (locally) on that specific hierarchy level.

[4]Discontinuities in $\dot{\hat{\boldsymbol{x}}}_i$ can lead to a discontinuous control law if the active damping on level i is velocity-dependent.

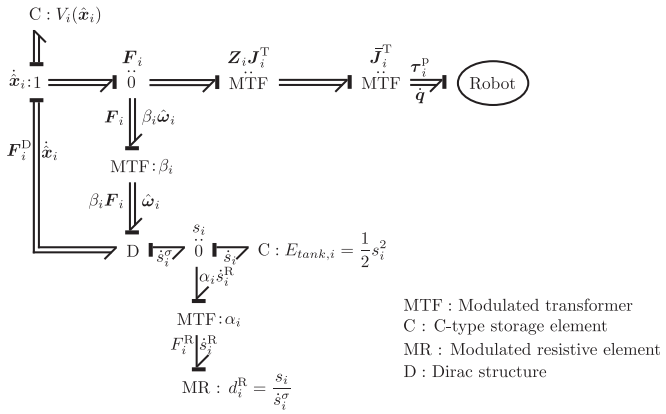

Fig. 2. Bond graph of the extended null space compliance controller with local energy tank on level $(2 \leq i \leq r)$. The notations follow [21].

depicts the energy flow. The Dirac structure D implements

$$\begin{pmatrix} \boldsymbol{F}_i^{\mathrm{D}} \\ \hat{\boldsymbol{w}}_i \\ -\dot{s}_i^{\sigma} \end{pmatrix} = \begin{pmatrix} \boldsymbol{0} & \boldsymbol{0} & \begin{pmatrix} \boldsymbol{D}_i\dot{\hat{\boldsymbol{x}}}_i \\ \hline s_i \end{pmatrix} \\ \boldsymbol{0} & \boldsymbol{0} & \begin{pmatrix} \hat{\boldsymbol{w}}_i \\ \hline s_i \end{pmatrix} \\ -\begin{pmatrix} \boldsymbol{D}_i\dot{\hat{\boldsymbol{x}}}_i \\ \hline s_i \end{pmatrix}^T & -\begin{pmatrix} \hat{\boldsymbol{w}}_i \\ \hline s_i \end{pmatrix}^T & 0 \end{pmatrix} \begin{pmatrix} \dot{\hat{\boldsymbol{x}}}_i \\ \beta_i\boldsymbol{F}_i \\ s_i \end{pmatrix} , \tag{17}$$

in which the force $\boldsymbol{F}_i^{\mathrm{D}} = \boldsymbol{D}_i\dot{\hat{\boldsymbol{x}}}_i$ is generated and the flow

$$\dot{s}_i^{\sigma} = \frac{1}{s_i}\left(\dot{\hat{\boldsymbol{x}}}_i^T\boldsymbol{D}_i\dot{\hat{\boldsymbol{x}}}_i + \beta_i\hat{\boldsymbol{w}}_i^T\boldsymbol{F}_i\right) \tag{18}$$

is defined. Eq. (18) determines the energy flow towards the virtual tank and has two components: the energy flow from the active damping on level i is unidirectional, while this is not the case for the second term, similar to the last term in (12). The introduction of $\dot{s}_i^{\sigma}$ is due to the constraint of limiting $E_{\mathrm{tank},i}$ by its maximum value $E_{\mathrm{tank},i}^{\max} \in \mathbb{R}^+$. The modulated transformer α_i in Fig. 2 can be interpreted as an *overflow valve*. As long as $E_{\mathrm{tank},i} < E_{\mathrm{tank},i}^{\max}$, energy exchange between the Dirac structure and the virtual energy tank is (unrestrictedly) permitted. But if $E_{\mathrm{tank},i} \geq E_{\mathrm{tank},i}^{\max}$ holds, then the complete energy flow towards the energy tank is dissipated through the modulated resistive element

$$d_i^{\mathrm{R}} = \frac{s_i}{\dot{s}_i^{\sigma}} \tag{19}$$

w.r.t. the corresponding flow-effort-pair

$$\dot{s}_i^{\mathrm{R}} = \alpha_i\dot{s}_i^{\sigma} \ , \ F_i^{\mathrm{R}} = \alpha_i s_i \ . \tag{20}$$

Herein, the overflow valve is switched according to the law

$$\alpha_i = \begin{cases} 1 & \text{if } (E_{\mathrm{tank},i} \geq E_{\mathrm{tank},i}^{\max}) \wedge (\dot{\hat{\boldsymbol{x}}}_i^T\boldsymbol{D}_i\dot{\hat{\boldsymbol{x}}}_i + \beta_i\hat{\boldsymbol{w}}_i^T\boldsymbol{F}_i > 0) \\ 0 & \text{else.} \end{cases} \tag{21}$$

The 0-junction next to the virtual energy tank fulfills the condition

$$\dot{s}_i = \dot{s}_i^{\sigma} - \alpha_i\dot{s}_i^{\mathrm{R}} = (1-\alpha_i^2)\dot{s}_i^{\sigma} \ , \tag{22}$$

which reflects the desired behavior: the energy tank can only be filled ($\dot{s}_i > 0$) if the overflow valve is closed ($\alpha_i = 0$). Otherwise, the fill level is retained ($\dot{s}_i = 0$).

D. Passivity Analysis

In the following, the formal proof of passivity is derived for the controller with local energy tanks. That includes the passivation on the subtask levels and the required passivity in case of physical interaction with the controlled robot.

1) Proof of Passivity for the Hierarchical Compliance Controller on Level i: The new storage function for the entire potential energy on subtask level $i = 2 \ldots r$ is

$$S_{\mathrm{pot},i} = V_i(\tilde{\hat{\boldsymbol{x}}}_i) + E_{\mathrm{tank},i} \ , \tag{23}$$

with the deviation $\tilde{\hat{\boldsymbol{x}}}_i$ of $\hat{\boldsymbol{x}}_i$ from the reference value. Using (22) and (18), its time derivative yields

$$\dot{S}_{\mathrm{pot},i} = -\dot{\boldsymbol{q}}^T\boldsymbol{\tau}_i^{\mathrm{p}} - \alpha_i^2(\dot{\hat{\boldsymbol{x}}}_i^T\boldsymbol{D}_i\dot{\hat{\boldsymbol{x}}}_i + \beta_i\hat{\boldsymbol{w}}_i^T\boldsymbol{F}_i) \leq -\dot{\boldsymbol{q}}^T\boldsymbol{\tau}_i^{\mathrm{p}} \tag{24}$$

since $-\alpha_i^2(\dot{\hat{\boldsymbol{x}}}_i^T\boldsymbol{D}_i\dot{\hat{\boldsymbol{x}}}_i + \beta_i\hat{\boldsymbol{w}}_i^T\boldsymbol{F}_i) \leq 0$ due to (21). From (24) one can conclude passivity of the extended null space compliance controller on level i w.r.t. the power port $(\dot{\boldsymbol{q}}, -\boldsymbol{\tau}_i^{\mathrm{p}})$. The practical consequence of the energy tank and the deliberate deviations $\hat{\boldsymbol{x}}_i - \boldsymbol{x}_i$ is that the closed loop can be regarded as an exclusive interconnection of passive subsystems, so that all active components in Fig. 1 get passive.

2) Proof of Passivity of the Decoupled Closed-Loop Dynamics and the Overall System Dynamics: The proof of passivity for the decoupled dynamics on all hierarchy levels $i = 1 \ldots r$ can be obtained by utilizing the storage function

$$S_i = \frac{1}{2}\boldsymbol{v}_i^T\boldsymbol{\Lambda}_i\boldsymbol{v}_i + S_{\mathrm{pot},i} \tag{25}$$

with $S_{\mathrm{pot},1} = V_1(\tilde{\boldsymbol{x}}_1)$. Accordingly, its time derivative yields

$$\dot{S}_i = \boldsymbol{v}_i^T\boldsymbol{F}_i^{\mathrm{ext}} + \dot{S}_{\mathrm{pot},i} + \dot{\boldsymbol{q}}^T\boldsymbol{\tau}_i^{\mathrm{p}} \leq \boldsymbol{v}_i^T\boldsymbol{F}_i^{\mathrm{ext}} \tag{26}$$

due to (24). From (26) one can conclude passivity of the decoupled, hierarchical dynamics on level i w.r.t. the external forces $\boldsymbol{F}_i^{\mathrm{ext}} \in \mathbb{R}^{m_i}$ (input) and the velocities $\boldsymbol{v}_i$ (output).

Moreover, one can even show passivity of the overall closed-loop dynamics w.r.t. the complete external torques $\boldsymbol{\tau}^{\mathrm{ext}}$ (input) and the joint velocities $\dot{\boldsymbol{q}}$ (output). That power port is more intuitive than the above-mentioned one with the external forces $\boldsymbol{F}_i^{\mathrm{ext}}$ as input, which have been defined in the unintuitive hierarchically decoupled null space of level i. One can design an overall storage function via

$$S = \sum_{i=1}^{r} S_i \ . \tag{27}$$

Due to (26) the time derivative of (27) fulfills

$$\dot{S} \leq \sum_{i=1}^{r} \boldsymbol{v}_i^T\boldsymbol{F}_i^{\mathrm{ext}} = \dot{\boldsymbol{q}}^T\boldsymbol{\tau}^{\mathrm{ext}} \tag{28}$$

and delivers the demanded proof of passivity. The practical consequence is that the hierarchical controller will *never* generate energy. This safety-critical feature is not provided by any classical null-space-based redundancy resolutions.

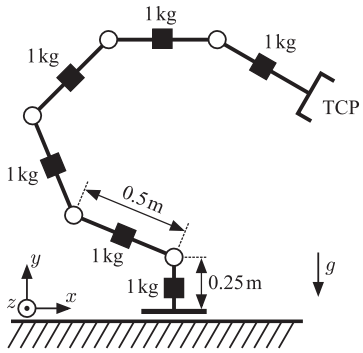

Fig. 3. Planar manipulator with 6 DOF used for the simulations. It contains one prismatic joint and five revolute joints. Each link is modeled as a massless bar with a point mass of 1 kg located in its middle. The leg length of the first link is 0.25 m, while all other links have a length of 0.5 m.

IV. Controller With Global Energy Tank

The concept in Section III passivates all subtask levels individually and keeps the dissipated energy from one level on this very level. While that conservative approach does not allow an exchange of energies across the priority levels, one might also think about one single energy tank for the entire hierarchy.

The controller design is very similar to the one in Section III and will not be detailed here. Instead of filling $r-1$ local energy tanks, the dissipated energy fills only one tank ($E_{\mathrm{tank,g}}$ with index "g" standing for "global") which can be tapped by all subtask controllers simultaneously. If the tank is empty, all subtask operational space coordinates will simultaneously deviate from the original values, i.e. $\beta_i = 0$ for $i = 2 \dots r$ in (14). This exchange of energies across the priority levels has influence on the passivity properties:

1) In contrast to (24), the null space compliance controllers do not feature individual, level-specific passive behavior.
2) In contrast to (26), passivity w.r.t. $\boldsymbol{F}_i^{\mathrm{ext}}$ (input) and $\boldsymbol{v}_i$ (output) is not provided on the individual subtask levels.

Nevertheless, overall passivity of the closed loop w.r.t. $\boldsymbol{\tau}^{\mathrm{ext}}$ (input) and $\dot{\boldsymbol{q}}$ (output) is still guaranteed similar to (28). In other words, one global energy tank is less conservative than several local energy tanks because all subtasks fill this global tank and can benefit from it at the same time. However, this exchange of energies across the hierarchy has to be paid by potential activity on single priority levels since the proof of passivity only covers the entire system and not the individual levels, in contrast to the local-tank case.

V. Simulations and Experiments

A. Simulations

A 6-DOF, planar manipulator is simulated which is sketched in Fig. 3. The task hierarchy consists of five priority levels:

1) Level 1 ($m_1 = 2$): Transl. Cart. impedance (TCP in x, y)
2) Level 2 ($m_2 = 1$): Rot. Cart. impedance (TCP about z)
3) Level 3 ($m_3 = 1$): Joint impedance (second joint)
4) Level 4 ($m_4 = 1$): Joint impedance (first joint)
5) Level 5 ($m_5 = 1$): Singularity avoidance (end-effector)

The corresponding task descriptions with initial and desired values as well as the controller gains are presented in Table I. Note that the lowest-priority-level task describes a unilateral constraint, i.e. the singularity avoidance only gets activated when the kinematic manipulability measure $m_{\mathrm{kin}}(\boldsymbol{q})$ falls below the specified value of 0.2.

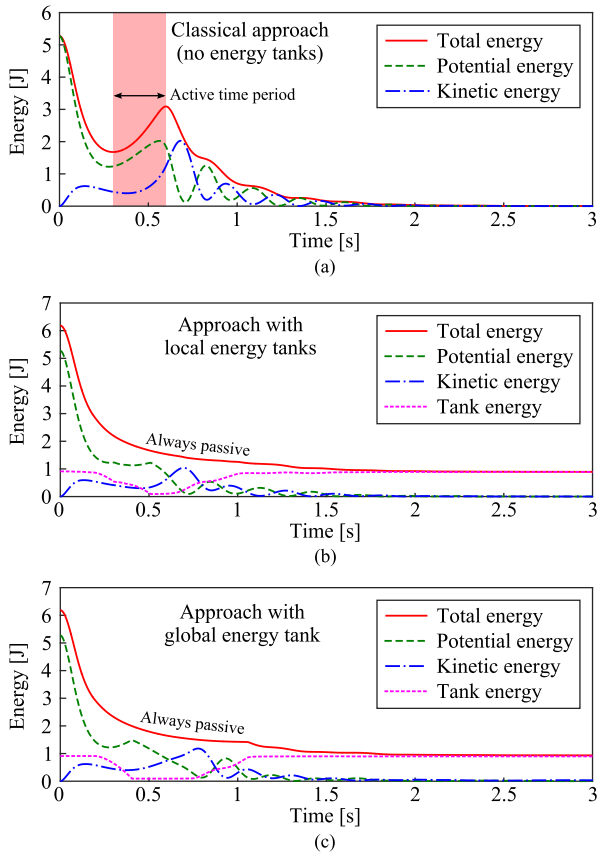

Fig. 4. Comparison of the energy contributions without energy tanks (top), with local energy tanks (center), and with one global energy tank (bottom).

The design parameters of the local energy tanks are given in the right columns of Table I: the initial tank energies $E_{\mathrm{tank},i}^{\mathrm{init}}$ and the upper limits $E_{\mathrm{tank},i}^{\mathrm{max}}$ are set to 25 % of the maximum total energy of the original, decoupled closed-loop system at the respective subtask level $i = 2 \dots 5$. Thus, the tank energy can only contribute little to the overall energy. The lower limits $E_{\mathrm{tank},i}^{\mathrm{min}}$ are set to 10 % of the initial tank energy. The global energy tank is both initialized and limited to $E_{\mathrm{tank,g}}^{\mathrm{init}} = E_{\mathrm{tank,g}}^{\mathrm{max}} = \sum_{i=2}^{5} E_{\mathrm{tank},i}^{\mathrm{init}}$ and can be tapped as long as $E_{\mathrm{tank,g}}^{\mathrm{min}} = \sum_{i=2}^{5} E_{\mathrm{tank},i}^{\mathrm{min}}$ is not fallen below.

The step responses for the classical solution and both energy tank approaches are shown in Fig. 4 in terms of the involved energies. No external forces are applied. The upper diagram highlights a time period (shaded area) in which energy is generated by the controller so that the total energy in the system increases. This active interval is completely avoided by means of energy tanks (center and lower diagram).

The errors in the operational spaces are depicted in Fig. 5. The comparison reveals that all approaches perform well and feature slightly different transients only. Since the restoration of the passivity has to be paid for, the convergence rate with the classical controller is marginally better. Nevertheless, it appears that overshooting is reduced when local tanks are implemented. The diagrams indicate the correct implementation of the hierarchy in all controllers. Higher-priority tasks are not disturbed

TABLE I
TASK DESCRIPTIONS AND CONTROLLER PARAMETERIZATION FOR THE SIMULATION

Priority	Task coord.	Initial val.	Goal val.	$\boldsymbol{K}_i$	$\boldsymbol{D}_i$	$\boldsymbol{K}_{\mathrm{P},i}$	$E^{\mathrm{init}}_{\mathrm{tank},i}$	$E^{\mathrm{max}}_{\mathrm{tank},i}$	$E^{\mathrm{min}}_{\mathrm{tank},i}$
Level 1	TCP in x	1.34 m	1.60 m	20 N/m	8 Ns/m	–	–	–	–
	TCP in y	2.29 m	1.80 m	20 N/m	8 Ns/m	–	–	–	–
Level 2	$\sum_{i=2}^{6} \boldsymbol{q}_i$	0.65 rad	1.20 rad	10 Nm/rad	0.7 Nms/rad	10 Nm/rad	0.378 J	0.378 J	0.038 J
Level 3	$\boldsymbol{q}_2$	−0.40 rad	−0.55 rad	40 Nm/rad	0.8 Nms/rad	10 Nm/rad	0.456 J	0.456 J	0.046 J
Level 4	$\boldsymbol{q}_1$	0.40 m	0.50 m	50 N/m	3.0 Ns/m	10 N/m	0.063 J	0.063 J	0.006 J
Level 5	$m_{\mathrm{kin}}(\boldsymbol{q})$	1.89	>0.2	100 if $m_{\mathrm{kin}}(\boldsymbol{q}) \leq 0.2$, 0 else	2.0	10	0.013 J	0.013 J	0.001 J

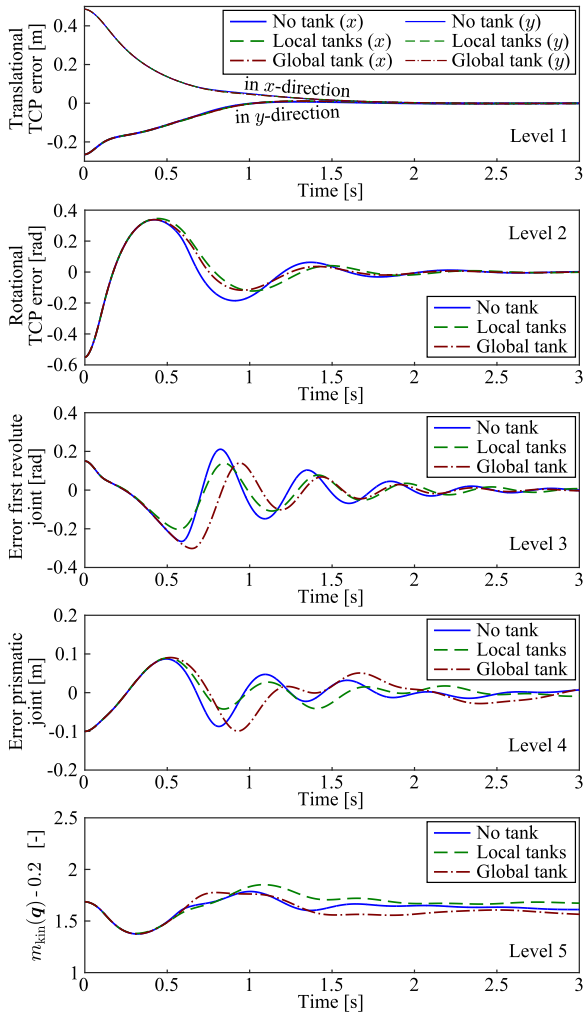

Fig. 5. Operational space errors on all priority levels for the three controllers.

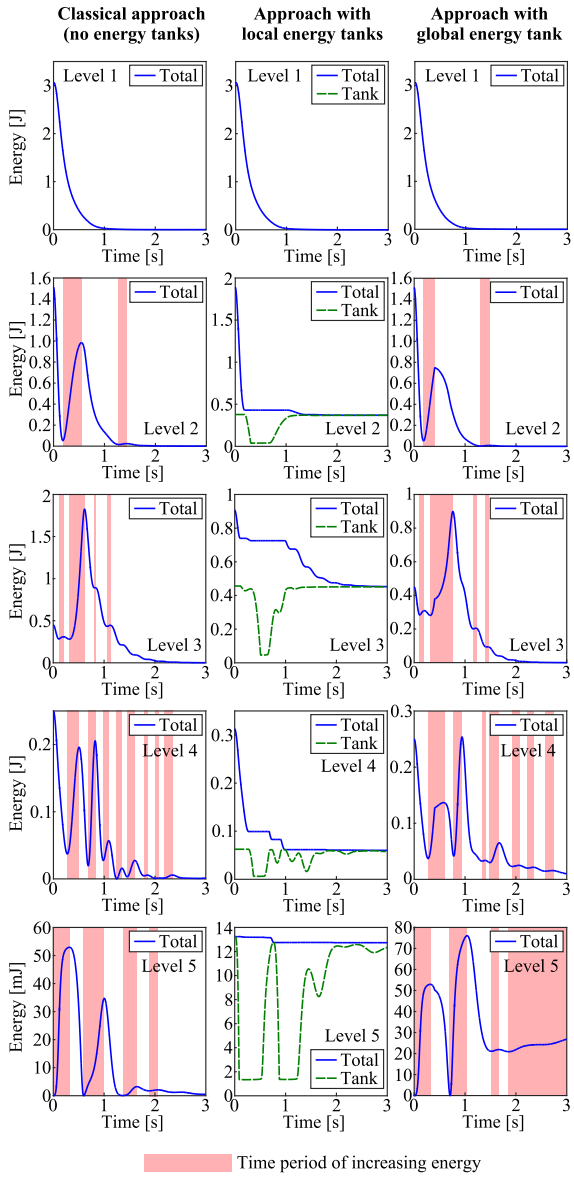

Fig. 6. Energies on all hierarchy levels: the left column depicts the classical approach, the center column shows the behavior with local energy tanks, and the right column represents the solution with one global energy tank.

by lower-priority ones but the other way round. Therefore, the following (expected) tendency can be deduced: the lower the priority level, the longer it takes to converge.

The comparison of the total energies on all individual hierarchy levels is provided by Fig. 6 column-wise. One can clearly see numerous time periods with increasing total energy on all subtask levels in the classical approach, marked by the shaded areas. Moreover, the global-energy-tank solution suffers from similar drawbacks since the controller does not ensure passivity on the individual subtask levels but only for the system as a whole (as already shown in Fig. 4). Only the local-energy-tank solution features passive behavior on all subtask levels and for the overall closed-loop system. The level-specific local tank energies are shown in the center-column diagrams to give an insight into the level-specific energy exchange and to indicate when the respective tank gets empty, i.e. the control performance deteriorates.

B. Experiments

The controllers have been implemented on the upper body of Rollin' Justin with 17 actuated DOF (left arm: 7, right arm: 7, torso: 3). Three priority levels are considered:

1) *Level 1: Cartesian impedance of both arms* ($m_1 = 12$) with $400\,\frac{\mathrm{N}}{\mathrm{m}}$ (translational stiffness), $20\,\frac{\mathrm{Nm}}{\mathrm{rad}}$ (rotational stiffness), and 0.7 as damping ratio in all modal directions.
2) *Level 2: Joint impedance of torso* ($m_2 = 3$) with $150\,\frac{\mathrm{Nm}}{\mathrm{rad}}$ (stiffness for vertical axis), $400\,\frac{\mathrm{Nm}}{\mathrm{rad}}$ (stiffness for horizontal axes), and 0.7 as damping ratio in all joints.
3) *Level 3: Joint impedance of upper body* ($m_3 = 17$) with the same torso stiffness/damping as on level 2, and $50\,\frac{\mathrm{Nm}}{\mathrm{rad}}$ as stiffness in each arm joint. The damping ratio is set to 0.7 in all joints.

The local energy tanks (29), (30) and the global energy tank (31) are parameterized as follows:

$$E_{\mathrm{tank},2}^{\mathrm{init}} = 0\,\mathrm{J}\,, E_{\mathrm{tank},2}^{\mathrm{max}} = \ 5\,\mathrm{J}\,, E_{\mathrm{tank},2}^{\mathrm{min}} = 2\,\mathrm{J} \tag{29}$$

$$E_{\mathrm{tank},3}^{\mathrm{init}} = 0\,\mathrm{J}\,, E_{\mathrm{tank},3}^{\mathrm{max}} = 10\,\mathrm{J}\,, E_{\mathrm{tank},3}^{\mathrm{min}} = 1\,\mathrm{J} \tag{30}$$

$$E_{\mathrm{tank,g}}^{\mathrm{init}} = 0\,\mathrm{J}\,, E_{\mathrm{tank,g}}^{\mathrm{max}} = 15\,\mathrm{J}\,, E_{\mathrm{tank,g}}^{\mathrm{min}} = 3\,\mathrm{J}. \tag{31}$$

The gains in the drift compensation are equal in both energy-tank controllers: $\boldsymbol{K}_{\mathrm{P},2} = \mathrm{diag}(5,5,5)\,\frac{\mathrm{Nm}}{\mathrm{rad}}$, $\boldsymbol{K}_{\mathrm{P},3} = \mathrm{diag}(5,\ldots,5)\,\frac{\mathrm{Nm}}{\mathrm{rad}}$. Four transients are recorded, with step commands at levels 1 and 2 (both consistent and feasible), whereas the reference on level 3 is kept constant (inconsistent with level 1 and 2). In the following diagrams, the times with changing setpoints are highlighted by shaded rectangles. The level-specific potential energies and the total system energy are plotted in Fig. 7. One can see that the performances on level 1 and 2 are very similar for all controllers. Level 3 illustrates larger differences. While the task energy with the classical approach increases massively, both energy tank approaches allow a deviation $\hat{\boldsymbol{x}}_3 - \boldsymbol{x}_3 \neq \boldsymbol{0}$ such that the springs are only loaded to an extent which still guarantees passivity. The result can be found in the bottom diagram of Fig. 7. Both energy-tank-concepts ensure passivity during the transients, while the classical approach leads to active time periods. Fig. 8 (bottom) illustrates the error in the original task spaces of level 3. Ensuring the passivity has to be paid by a slightly deteriorated control performance. As expected, the best performance is achieved with the original control law. Moreover, using a global energy tank leads to a higher performance than a local one. This aspect will be discussed in Sect. VI. The introduced deviations $\|\hat{\boldsymbol{x}}_2 - \boldsymbol{x}_2\|_2$ and $\|\hat{\boldsymbol{x}}_3 - \boldsymbol{x}_3\|_2$ are presented in Fig. 8 (upper two diagrams). While the deviations on level 2 are negligible ($<$0.031 rad), the coordinates deviate largely on level 3 in order to preserve the passivity. These level-3 deviations evidently comply with the behavior shown in the third diagram of Fig. 7.

VI. Discussion

In Fig. 4, one could see that the increase of the total energy in the classical approach is significantly higher than the maximum tank energy in both new controllers. The tanks serve as buffers, and if empty, further undesired, "increasing" energy will be directly dissipated by reducing the control performance. Therefore, one can consider both the local energy tank solution

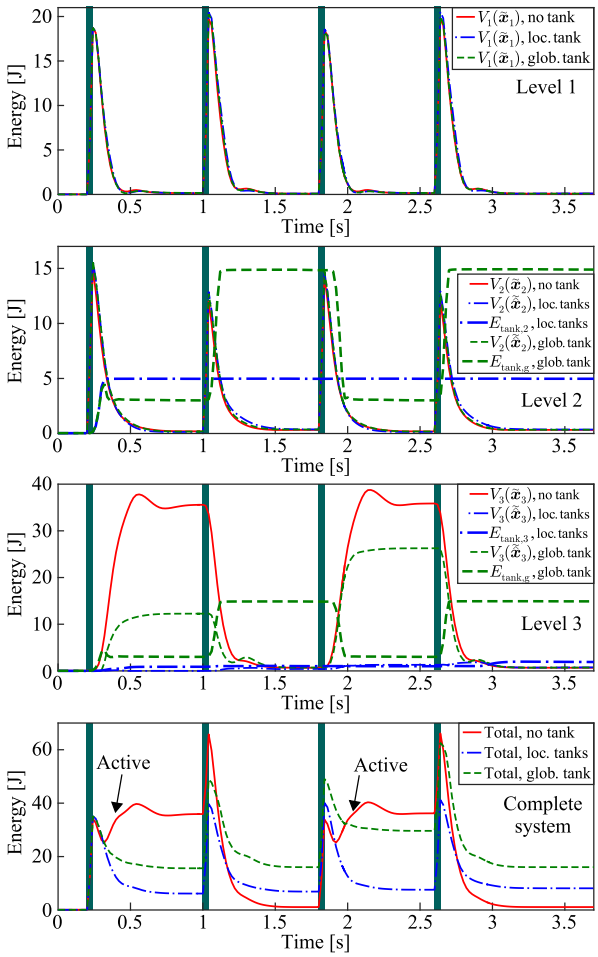

Fig. 7. Level-wise potential energies and total energies for all controllers.

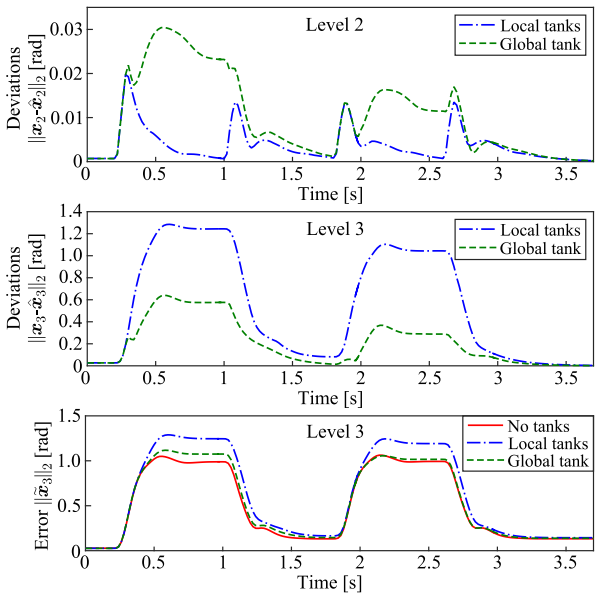

Fig. 8. Deviations between the original and new coordinates for $i = 2, 3$ (upper two diagrams) and errors in the original task space of level 3 (bottom).

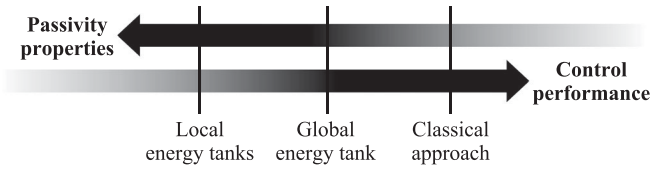

Fig. 9. Qualitative classification of the controllers.

and the global energy tank concept as safety features that keep the high control performance as long as possible and modify the control law only if unavoidable. As soon as possible, the high performance is completely recovered.

A great danger in classical controllers is that the potential energy of a subordinate, unfeasible task grows and leads to huge task torques. These torques are then filtered by the null space projectors, i.e. they do not affect the control action. However, if the null space projectors change, e.g. due to joint motions, these critical task torques may suddenly lead to instability after being null-space-projected. If the energy tanks are empty or properly upper-bounded in the approaches proposed here, *these issues cannot occur at all* because the deviations $\hat{\boldsymbol{x}}_i - \boldsymbol{x}_i$ in the task coordinates $i = 2 \dots r$ prevent such increasing task torques from the beginning.

One should note that the control law does not require any force measurements. Therefore, no problems in terms of time delays of such signals exist. All feedback terms are computed based on the measured states $\boldsymbol{q}$ and $\dot{\boldsymbol{q}}$.

Which differences exist between the approaches with local energy tanks and global energy tank? Both controllers ensure overall passivity in contrast to the classical approach (cf. Fig. 4). Yet, only the local tanks guarantee passivity on each hierarchy level individually (cf. Fig. 6), whereas the global tank can "mask" poor performance on single levels (oscillations, temporary activity, etc.). However, since the tanks are locally placed, there is no energy exchange across the priority levels, which is more conservative in general. That characteristic has also been observed in the experiments, see Fig. 8 (bottom). A qualitative classification of the three controllers is given in Fig. 9. Therein the *control performance* is defined as follows: the less additional control intervention to achieve specific passivity properties, the higher the control performance.

Summarized one can say that the choice of the controller is highly dependent on the application. To be on the safe side, one chooses the controller with local energy tanks. To achieve the best performance, the classical controller fits best. Also note that a formal proof of stability based on semi-definite Lyapunov functions can be found even in the classical approach [17]. The use of a global energy tank is an adequate trade-off between these border cases.

VII. Conclusion

A generic approach has been presented to passivate multi-objective torque control with an arbitrarily complex task hierarchy. The concept utilizes virtual energy tanks to modify the energy flows in the system (in two variations): local energy tanks on each hierarchy level and one global energy tank for the entire hierarchy. Both controllers have been compared with each other and the classical, non-passive approach in theory, simulations, and experiments. The new approaches provide high control performance as long as possible, and, only if unavoidable, reduce it to preserve the passivity in any case. They extend the repertoire of hierarchical controllers for safety-relevant applications, where physical interaction with the environment is required.

References

[1] Y. Nakamura, H. Hanafusa, and T. Yoshikawa, "Task-priority based redundancy control of robot manipulators," *Int. J. Robot. Res.*, vol. 6, no. 2, pp. 3–15, 1987.

[2] O. Khatib, "A unified approach for motion and force control of robot manipulators: The operational space formulation," *IEEE J. Robot. Autom.*, vol. RA-3, no. 1, pp. 43–53, Feb. 1987.

[3] B. Siciliano and J.-J. Slotine, "A general framework for managing multiple tasks in highly redundant robotic systems," in *Proc. Fifth Int. Conf. Adv. Robot. 'Robots Unstructured Environments*, 1991, pp. 1211–1216.

[4] A. Dietrich, C. Ott, and S. Stramigioli, "Passivation of projection-based null space compliance control via energy tanks," *IEEE Robot. Autom. Lett.*, vol. 1, no. 1, pp. 184–191, Jan. 2016.

[5] S. Stramigioli, "Energy-aware robotics," in *Mathematical Control Theory I*, (ser. Lecture Notes in Control and Information Sciences 461), M. K. Camlibel, A. A. Julius, R. Pasumarthy, and J. M. A. Scherpen, Eds. New York, NY, USA: Springer, 2015, ch. 3, pp. 37–50.

[6] C. Secchi, A. Franchi, H. H. Bülthoff, and P. R. Giordano, "Bilateral teleoperation of a group of UAVs with communication delays and switching topology," in *Proc. 2012 IEEE Int. Conf. Robot. Autom.*, 2012, pp. 4307–4314.

[7] D. Lee and K. Huang, "Passive-set-point modulation framework for interactive robotic systems," *IEEE Trans. Robot.*, vol. 26, no. 2, pp. 354–369, Apr. 2010.

[8] M. Franken, S. Stramigioli, S. Misra, C. Secchi, and A. Macchelli, "Bilateral telemanipulation with time delays: A two-layer approach combining passivity and transparency," *IEEE Trans. Robot.*, vol. 27, no. 4, pp. 741–756, Aug. 2011.

[9] A. Franchi, C. Secchi, H. I. Son, H. H. Bülthoff, and P. R. Giordano, "Bilateral telemanipulation of groups of mobile robots with time-varying topology," *IEEE Trans. Robot.*, vol. 28, no. 5, pp. 1019–1033, Oct. 2012.

[10] C. Secchi, S. Stramigioli, and C. Fantuzzi, "Position drift compensation in Port–Hamiltonian based telemanipulation," in *Proc. 2006 IEEE/RSJ Int. Conf. Intell. Robot. Syst.*, 2006, pp. 4211–4216.

[11] F. Ferraguti, C. Secchi, and C. Fantuzzi, "A tank-based approach to impedance control with variable stiffness," in *Proc. 2013 IEEE Int. Conf. Robot. Autom.*, 2013, pp. 4948–4953.

[12] F. Ferraguti *et al.*, "An energy tank-based interactive control architecture for autonomous and teleoperated tobotic surgery," *IEEE Trans. Robot.*, vol. 31, no. 5, pp. 1073–1088, Oct. 2015.

[13] T. S. Tadele, T. J. de Vries, and S. Stramigioli, "Combining energy and power based safety metrics in controller design for domestic robots," in *Proc. 2014 IEEE Int. Conf. Robot. Autom.*, 2014, pp. 1209–1214.

[14] C. Schindlbeck and S. Haddadin, "Unified passivity-based Cartesian force/impedance control for rigid and flexible joint robots via task-energy tanks," in *Proc. 2015 IEEE Int. Conf. Robot. Autom.*, 2015, pp. 440–447.

[15] K. Kronander and A. Billard, "Passive interaction control with dynamical systems," *IEEE Robot. Autom. Lett.*, vol. 1, no. 1, pp. 106–113, Jan. 2016.

[16] A. Dietrich, *Whole-Body Impedance Control of Wheeled Humanoid Robots*, (ser. Springer Tracts in Advanced Robotics), vol. 116. New York, NY, USA: Springer, 2016.

[17] C. Ott, A. Dietrich, and A. Albu-Schäffer, "Prioritized multi-task compliance control of redundant manipulators," *Automatica*, vol. 53, pp. 416–423, 2015.

[18] A. Dietrich, C. Ott, and A. Albu-Schäffer, "An overview of null space projections for redundant, torque-controlled robots," *Int. J. Robot. Res.*, vol. 34, no. 11, pp. 1385–1400, 2015.

[19] N. Hogan, "Impedance control: An approach to manipulation: Part I—Theory, Part II—Implementation, Part III—Applications," *J. Dyn. Syst. Meas. Control*, vol. 107, pp. 1–24, 1985.

[20] P. R. Giordano, A. Franchi, C. Secchi, and H. H. Bülthoff, "A passivity-based decentralized strategy for generalized connectivity maintenance," *Int. J. Robot. Res.*, vol. 32, no. 3, pp. 299–323, 2013.

[21] W. Borutzky, *Bond Graph Methodology: Development and Analysis of Multidisciplinary Dynamic System Models*. New York, NY, USA: Springer Science & Business Media, 2009.